Physica C: Superconductivity and its applications 632 (2025) 1354694

Contents lists available at ScienceDirect

Physica C: Superconductivity and its applications

journal homepage: www.elsevier.com/locate/physc

Full length article

Thermal transmittance measurements of niobium at cryogenic temperatures

Marc Wenskat [a,b,*], Leon King [a], Lasse Koch [a], Cem Saribal [a], Anton Lorf [a], Isabel González Díaz-Palacio [a], Cornelius Martens [a], Robert Zierold [c], Wolfgang Hillert [a]

[a] Institute of Experimental Physics, University Hamburg, Germany
[b] Deutsches Elektronen-Synchrotron DESY, Germany
[c] Institute for Nanostructure and Solid State Physics, University Hamburg, Germany

ARTICLE INFO

Keywords:
Superconductor
Niobium
Thermal conductance

ABSTRACT

The first $\mathcal{O}(100\,\mathrm{nm})$ of the inner surface Niobium-based superconducting RF (SRF) cavities are crucial to achieve high accelerating fields and a low surface resistance. Recent treatments aim to improve superconducting properties by tailoring the interstitial atom concentration or by depositing thin superconducting films. Yet, no investigation of the thermal characteristics of those surfaces after such treatments has been done, although this is a crucial property to cool the induced RF losses away and to maintain the superconducting state while high surface magnetic fields are applied. In this contribution, a newly developed experimental set-up is described, which allowed the first ever measurement of the thermal transmittance of Mid-T heat treated and Superconductor-Insulator-Superconductor (SIS) coated niobium samples. The results show that the SIS samples perform the same as standard niobium and that Mid-T heat treated samples have an improved thermal transmittance of 30%.

1. Introduction

Particle accelerators play a crucial role in various research domains, where superconducting radio frequency (SRF) cavities are the backbone of these machines. To enhance their operational efficiency, a continuous effort is necessary to improve the SRF cavities to achieve higher accelerating fields and minimize RF losses.

Ensuring stable cavity operation entails effectively dissipating Joule heating, which is typically generated within the cavity walls, to an external helium bath. Consequently, there is considerable interest in experimentally assessing the impact of current and prospective cavity treatments on thermal characteristics. High thermal conductivity and low Kapitza resistance are important to achieve thermal stability, especially in the case of defects on the surface, and the behavior of the thermal properties after various treatments has already been shown to have a severe impact on overall RF performance [1–5].

All newly developed surface treatments of cavities intend to improve the superconducting properties but will also affect the thermal conductivity. In general, these two properties pull in opposite directions. This is because a superconductor is intrinsically a bad thermal conductor because some of the (electrical and thermal) conduction electrons are paired into Cooper pairs and thus cannot contribute anymore to the heat transfer.

Initial tests were performed to commission a newly established and described system, based on an earlier design [6], and to check if the values obtained are in agreement with known thermal transmittance values of niobium and determine its ability to detect changes due to surface treatments. The next step was then to apply new treatments and assess their impact onto the thermal transmittance. In this work, we present the results of the thermal performance evaluation of the SRF cavity materials under cryogenic conditions.

2. Experimental set up

To gain experimental insights into the thermal conductance of a given solid, it is necessary to induce a heat flux through it in a controlled manner and measure the resulting temperature gradient across it in an equilibrium condition. As the treatments we intend to study are only affecting the near surface of less than 1 µm, standard thermal conductance measurements are not feasible as they only measure bulk heat transportation on samples with a thickness of $\mathcal{O}(mm)$ and/or not at cryogenic temperatures. Hence, for the systematic sample study of thin films at cryogenic temperatures, a new experimental set-up is needed. Such a set-up has been developed already elsewhere but no longer exists [6]. Therefore, a new system, based on the earlier design, was built, which enforces the heat flux through the affected thin layer [7].

* Corresponding author at: Deutsches Elektronen-Synchrotron DESY, Germany.
E-mail address: marc.wenskat@desy.de (M. Wenskat).

https://doi.org/10.1016/j.physc.2025.1354694
Received 17 November 2024; Received in revised form 4 March 2025; Accepted 5 March 2025
Available online 12 March 2025

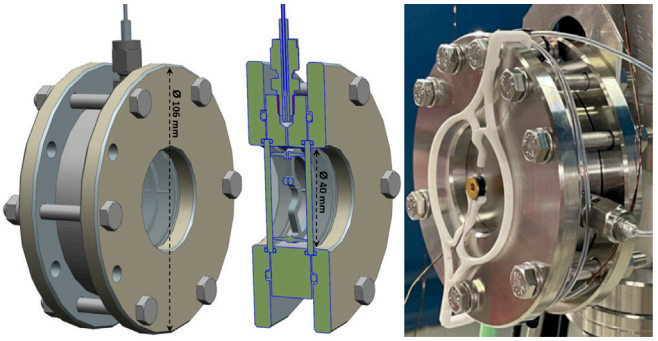

Fig. 1. Left shows the 3D view of the final design and a cross section view (center), where the filling capillary is shown at the top. The right image shows one of the cells installed at an insert. The 3D printed holder for the outer temperature sensor can be seen as well.

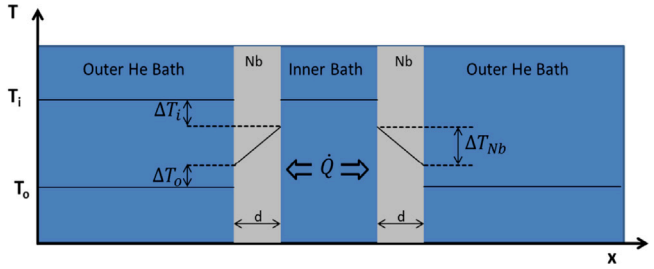

Fig. 2. Principle and temperature profile of the experiment. Note that $\Delta T_{Nb} = d \cdot \frac{\dot{Q}}{2\lambda A}$ and $\Delta T_{i,o} = R_k \cdot \frac{\dot{Q}}{2A}$.

2.1. Measurement principle

The new set-up is a superfluid helium leak-tight container with two identical study sample disks mounted on either sides of a cylindrical support made of stainless steel with a helium-solid interface of area A, see Fig. 1. A wire heater and a thermometer are installed inside the cell. The cell is placed in a superfluid helium-4 bath. The cell cavity is also filled with superfluid helium via a long capillary to transport the heat from the heater to the sample surface. Under steady-state conditions, a temperature jump ΔT is established between the He-bath temperature T_o and the temperature inside the cavity T_i, for different heat fluxes – see Fig. 2 for the measurement principle. The temperature jump ΔT and the heat flux $\dot{Q}$ are related as follows:

$$\left(\frac{d}{2\lambda} + R_K\right)\dot{Q} = A \cdot \Delta T = A\left(T_i - T_o\right) \tag{1}$$

where d is the sample disk thickness, λ the thermal conductivity, A the cross section through which the heat diffuses, and R_K the thermal interface resistance or Kapitza Resistance from the material to Helium. We further define the thermal transmittance K as

$$K = \left(\frac{d}{2\lambda} + R_k\right)^{-1} \tag{2}$$

as this value is obtained from this measurement. Shown in Fig. 3 is a typical measurement.

2.2. Uncertainty discussion

2.2.1. Statistical uncertainty

The temperature is measured using Lakeshore Cryotronics Cernox 1030 HT sensors in CU package, calibrated in the range of 1.4–325 K and the readout is done with the Lake Shore Cryogenic Temperature Controller Model 336. The measurement accuracy for the combined system is better than ±8.8 mK below 4.2 K. The heater is a 0.1 mm CuMn12Ni wire, wrapped around a 3D printed holder, which also

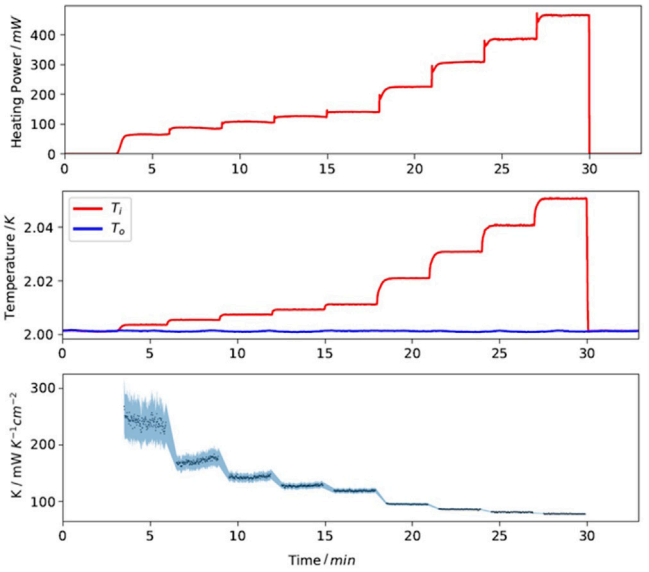

Fig. 3. The upper plot shows the applied heater power P, the middle plot shows the temperature inside T_i and outside T_o of the cell, and the bottom plot shows the obtained thermal transmittance for each step as a function of time. The black dots are the calculated values, the blue region shows the 1σ uncertainty. A measurement takes on average 30 min. This measurement is at 2 K.

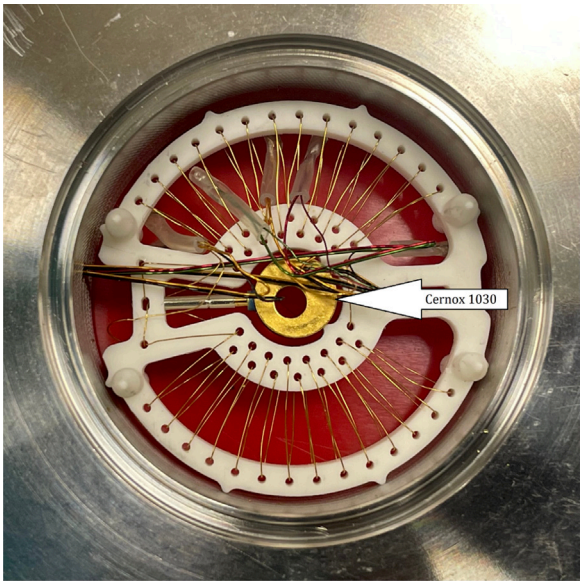

Fig. 4. Image of heating element and temperature sensor, indicated by the arrow, inside the measurement cell. The heating element consists of a Manganin wire wound inside of a 3D printed custom fixture, which also holds the temperature sensor in place. Four pins on each side of the fixture keep the electrical components centered between the samples.

contains the inner temperature sensor, see Fig. 4. The heater power is adjusted to a relative accuracy of 8% based on the accuracy of the controller for the heater current and voltage.

The uncertainty for each data point in the thermal transmittance measurement is calculated by propagation of error, see the blue regions for each data point in the bottom plot of Fig. 3.

The fit is done using a least square fitting with SciPy v1.11.3 [8], which takes the uncertainties of the thermal transmittance and the heater power as weights into account. The resulting uncertainty of the thermal transmittance K is then used as the statistical uncertainty of this result, and is typically on the order of 1%–2%.

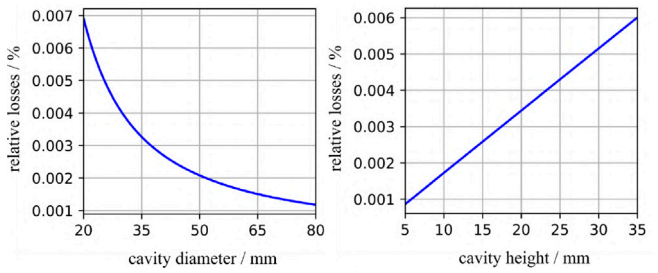

Fig. 5. Left: Relative heat loss $\dot{Q}_{cyl,rel}$ through the steel enclosure as function of sample diameter for a steel wall thickness of 20 mm and an inner cavity height of 16 mm. Right: Relative heat loss $\dot{Q}_{cyl,rel}$ through the steel enclosure as function of sample diameter for a seel wall thickness of 20 mm and a sample diameter of 40 mm.

2.2.2. Design optimization and systematic uncertainty

In an ideal set-up, the heat should flow only through the samples. In the real world, however, the heat can also take other paths from the inner helium bath to the outer one. A systematic discussion of the various paths needs to consider the heat through the steel enclosure, the filling capillary and the wire to the temperature sensor, and the analysis will be done in the similar way as in [6]. The stainless steel enclosure is reduced to a single part: a hollow cylinder that touches the niobium samples at its inner edges. From here on one can obtain the relative rate of heat flow through the stainless steel enclosure and optimize the Nb sample geometry and the steel enclosure to minimize the unwanted heat flow. Beneficial in this optimization is the significantly lower thermal conductivity of steel at cryogenic temperatures. From here on one can obtain the relative rate of heat flow through the stainless steel support $\dot{Q}_{cyl,rel}$ with

$$\dot{Q}_{cyl,rel} = \frac{\dot{Q}_{cyl}}{\dot{Q}_{cyl} + \dot{Q}_{sample}} \tag{3}$$

where $\dot{Q}_{sample}$ is the heat flow through both samples and $\dot{Q}_{cyl}$ the heat flow through the stainless steel cylinder. Starting with Fourier's law, one obtains the finale expression for the relative heat flow

$$\dot{Q}_{cyl,rel} = \frac{1}{1 + \frac{\lambda_{sample} d^2_{sample}}{4\lambda_{cyl} h_{cyl} h_{sample}} ln(\frac{d_{cyl}}{d_{sample}})} \tag{4}$$

which only depends on geometrical dimensions of the steel cylinder and the samples and the respective thermal conductivities. So by carefully considering and adjusting the dimensions of the instrument, one achieves accurate thermal conductance measurements while maintaining a practical size for real-world application - see Fig. 5 for the optimization. As the sample thickness h_{sample} was given by the sheet itself, the chosen dimensions were h_{cyl} = 16 mm and d_{sample} = 40 mm, which in our case resulted into a relative heat flow of 0.3%. The filling capillary is necessary to fill the inner volume of the cell with liquid helium, but needs to be long enough to decouple the inner helium bath thermally from the outer bath. To effectively minimize heat losses through the helium filling line capillary, a simple strategy is to reduce its inner diameter as much as possible. In this context, opting for a diameter of 1 mm is a well-considered decision, allowing for the smooth passage of all cables of the inner electronics while simultaneously mitigating heat losses. The filling line, being composed of superfluid helium, has a relatively high thermal conductivity, making it the most significant intrinsic heat loss source. Despite this, estimations reveal that losses through this capillary are kept below 5%. Likewise, the contributions of heat losses originating from the copper wiring have been assessed and found to be less than 0.05%. All estimates agree well with the same in-depth discussion of the previous device from Amrit et al. [6]. The final design is shown in Fig. 1.

2.2.3. Impact of leaks

The system will not be leak-tight against superfluid helium. Base on work done by Jergel et al. [9], it is possible to estimate the upper limit of heat which will be transported through a leak. Assuming that the samples are not sealed perfectly against the stainless steel cylinder, but a gap of 0.3 mm exist for the whole circumference, and using the maximum heat flux of 70 $\frac{\mathrm{mW}}{\mathrm{cm}^2}$ which can be transferred across such a gap before boiling occurs, a total heat of ≈60 mW can be transported away this way. For small heater powers, the heat flowing through the leak can be a significant share of up to 50% of the total heat flux, where the other share goes through the sample. As the flux through the leak is a fixed, an increase of the heater power will reduce the leak contribution to the total thermal transmittance and would be about up to 11% at the maximum heater power, see Fig. 3. Hence, at low powers the thermal transmittance is overestimated, while the value would converge toward the *true* value of the sample under investigation with higher heater powers as the share of the leak contribution becomes negligible. In addition, the heat transport through small leaks or channels shows a self-limiting behavior [10]. As the energy density in small channels increase, the helium losses is superfluid state and thermal conductance decreases significantly, leading to bubble formation which can effectively seal a leak if it is small enough. The critical energy density at which this effect seals the leak depends on the dimensions of the channel. In both cases, a fixed value and/or self-limiting behavior, a converging behavior is expected, and theory suggests a dependency as

$$K(\dot{Q}) = K_0 + a \cdot \left(\frac{\dot{Q}}{\dot{Q}_0}\right)^n \tag{5}$$

with a and n being phenomenological parameters, describing the system, K_0 the thermal transmittance of the sample, and $\dot{Q}_0$ the normalization. This normalization can be chosen arbitrary, but is chosen in such way, that $K(\dot{Q}_0) = 1.01 K_0$ for a better visualization.

This converging behavior was in fact observed in all measurements. The curves were fitted with the function from Eq. (5), and the thermal transmittance K_0 is used in the discussion.

In conclusion of this section, the statistical uncertainty is well below the systematical uncertainty. The total uncertainty for the thermal transmittance K_0 can be estimated to be on the order of 2% for the statistical uncertainty and an upper limit of 12% for the systematical uncertainty, coming from the cell design and the impact of leaks. The error bars shown in the plot will be the statistical uncertainty based on the propagation of error, while the uncertainty of measured values in the text will be the sum of statistical and systematic uncertainty.

3. Sample preparation

The samples used for the study were cut out of a single niobium sheet from the European XFEL cavity production where the sheet was produced by Plansee SE. The use of a single sheet from a vendor was motivated by the fact, that vendor depended thermal properties exist, stemming from the fabrication process and varying impurity content of the material [11]. Water jet cutting was used to get a total of 25 samples, 45 mm in diameter, with a thickness of 2.6 mm. Due to the sealing surface at the edges of the sample, the effective area through which the heat can diffuse has a diameter of 40 mm. An overview of the tested sample pairs is given in Table 1. In total three different treatments were studied, the European XFEL recipe, further dubbed *baseline*, the coating of the Nb samples with an insulating/superconducting multilayer structure called *SIS*, and a medium temperature heat treatment called *Mid-T*, which are further outlined in the following paragraph.

3.1. Baseline

To mimic the cavity surface analog to the European XFEL cavity procedure, all samples underwent a coarse buffered chemical polishing (BCP) of 130 µm and an outgassing annealing of 3 h at 800 °C in a pressure which was always better than 10^{-6} mbar [12,13]. The BCP was carried out with samples placed in a large acid bath. In between the samples, a small magnetic stirring pill was placed. The tank was then filled up with a BCP mixture, which had a temperature of 10 °C, and the stirrer was rotated to carry away the material dissolving from the niobium surface to ensure more uniform polishing. For the first BCP, which was sample pair 2, a thermal runaway occurred, leading to stronger etching and higher hydrogen uptake. For the subsequent surface removal, the BCP was placed within an ice-cooled bucket, and when the bath temperature reached 23 °C, the current mixture was replaced with a fresh, cool one—effectively removing the total layer in two steps. The subsequent outgassing annealing was then done in an UHV furnace to remove hydrogen incorporated due to the chemical polishing [14]. This is the baseline treatment for all samples.

3.2. SIS coating

One such treatment under investigation is the so-called Multilayer or Superconductor-Insulator-Superconductor (SIS) approach. The theory suggests, that by coating an alternating multilayer of insulator and superconductor with a T_c higher than niobium, where each film is thinner than the London penetration depth, it is possible to achieve accelerating fields and surface losses outperforming bulk niobium [15,16]. Our own and other groups have already succeeded in coating such films onto samples [17,18], but the impact of those films onto the thermal transmittance has not been studied yet. Especially the introduction of several thermal interfaces and hence an increased thermal interface resistance by this approach was seen as potentially problematic. This is due to the fact that it has been reported, that the thermal interface resistance of thin Nb films on Cu is a severe limitation for the RF performance [19], and therefore such multilayer systems needs to be investigated. Furthermore, up to our knowledge, there are no literature values for the thermal conductance of those materials available at 2 K. Our approach is to coat samples and cavities using Plasma-Enhanced Atomic-Layer-Deposition (PEALD) with layers of AlN and NbTiN as insulator and superconductor. To achieve a high T_c of 15.9 K, an anneal of our deposited NbTiN-film at 900 °C for 1 h is necessary [18]. Hence, we measured the thermal transmittance after deposition and after the anneal, to see if the increase of interfaces or the thermal conductance of NbTiN or AlN reduces the thermal characteristics of the SIS structure compared to bare niobium. To further increase any effect, both sides of the sample were coated with 15 nm AlN and 60 nm NbTiN.

3.3. Mid-T heat treatment

A recent heat treatment called *Mid-T* is a 3 h annealing with a plateau of 250–400 °C in vacuum [20–23]. This heat treatment significantly reduces the surface losses, and even shows an inverted dependency of the surface losses from the applied field. The research of the underlying mechanism will not be addressed here, but it has been shown that a significant uptake of oxygen into the niobium is evident [24,25], as the native niobium oxide will dissociate in that temperature range [26,27]. This oxide incorporation in the niobium will change the mean free path and the residual resistivity ratio (RRR) in a significant layer, and will therefore also change the thermal conductivity λ as shown by the heuristic equation below [28].

$$\lambda = \frac{RRR}{4}\bigg|_{4.2\,\mathrm{K}} \left[\mathrm{Wm^{-1}\,K^{-1}}\right]. \tag{6}$$

As the RRR is a dimensionless number it is necessary to provide the correct units to obtain the thermal conductivity. On the other hand, it has been reported that the Kapitza resistance of intentionally oxidized niobium cavities decreased, which lead to a higher quality factor during testing [4]. A recent study has been shown, that an optimal surface roughness exists, at which a resonant phonon trapping occurs, which leads to an enhanced heat transfer across the solid/superfluid interface [29,30]. As the reported oxide layer growth has lead to a higher surface roughness, it is possible that the observed reduction in the Kapitza resistance stems from this effect. This is also relevant for Mid-T heat treated cavities, as the oxide layer in its composition and thickness after annealing differs from the pre-annealing state [23,31,32] and could therefore also alter the Kapitza resistance.

Hence, we annealed a sample pair using the Mid-T heat treatment recipe in the UHV furnace at 300 °C for 3 h and measured the thermal transmittance before and after the heat treatment.

Table 1
Overview of sample pairs measured and in which state.

Sample pair	Status
1	As-fabricated
2	As-fabricated
6	Baseline 1
3	Baseline 2
5	Baseline 3
4	Baseline 4
5	Mid-T heat treated
2	SIS as-deposited
2	SIS annealed

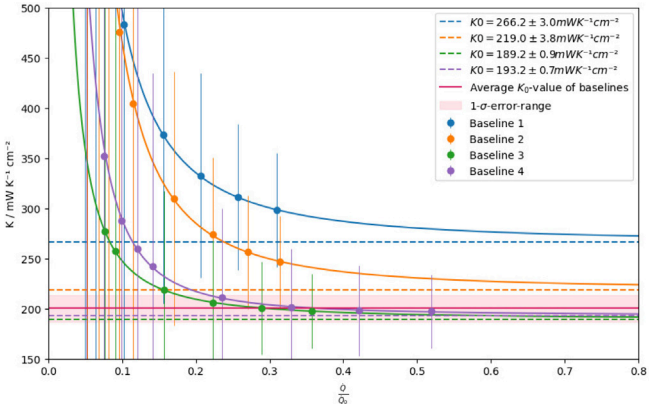

Fig. 6. Thermal transmittance K vs. normalized heat flux. The datapoints are the measurements, the lines the fit according to Eq. (5). The converged values for K_0 are given in the legend for each fit, the error bars are the 1σ confidence interval. The obtained thermal transmittance is in agreement with other literature values [3,35] for coarse BCP and subsequent outgassing annealing of 3 h at 800 °C. The average baseline is calculated omitting baseline 1 (see text below).

4. Results

The cell is installed parasitically at an insert which is then lowered into one of the vertical cryostats at the Accelerator Module and Test Facility (AMTF) at DESY [33,34]. After the cooldown and the subsequent test of the cavity installed in the insert is done, the thermal conductance measurements of the samples are done at 2 K and 1.8 K, where only the 2 K results are shown here. An overview of the results is given in Table 2

4.1. Nb baseline

The first measurements were done on two sample pairs, number 1 and 2, cut directly from the sheet without any further treatment. The obtained thermal transmittance is $(371 \pm 0.6\,(\mathrm{stat.}) \pm 36\,(\mathrm{sys.}))\,\mathrm{mW\,K^{-1}\,cm^{-2}}$ and $(401 \pm 0.7\,(\mathrm{stat.}) \pm 39\,(\mathrm{sys.}))\,\mathrm{mW\,K^{-1}cm^{-2}}$ respectively. Four

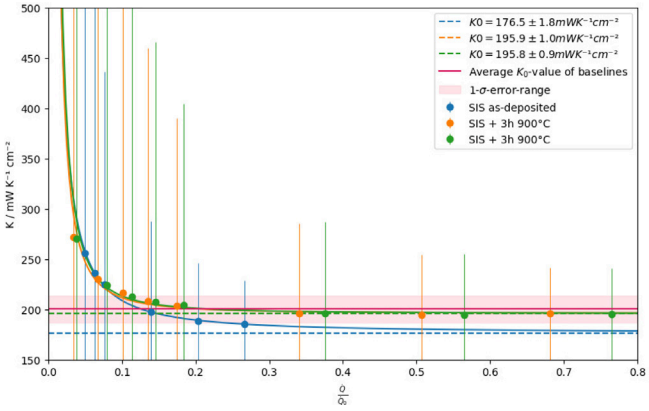

Fig. 7. Thermal transmittance K vs. normalized heat flux. The datapoints are the measurements, the lines the fit according to Eq. (5). The converged values for K_0 are given in the legend for each fit, the error bars are the 1σ confidence interval. No change compare to bare niobium is observed.

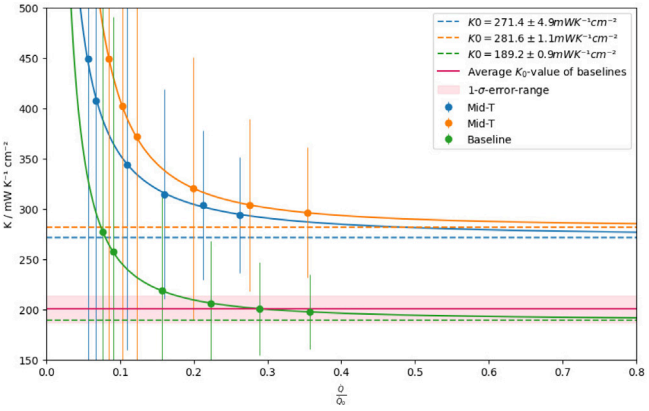

Fig. 8. Thermal transmittance K vs. normalized heat flux. The data points are the measurements, the lines the fit according to Eq. (5). The converged values for K_0 are given in the legend for each fit, the error bars are the 1σ confidence interval. A significant increase of the thermal transmittance is obvious.

sample pairs, number 3,4,5 and 6, were measured after the coarse BCP and the outgassing annealing of 3 h at 800 °C. These results are shown in Fig. 6. The first observation is that the thermal transmittance after the chemistry plus annealing is lower than the as-fabricated value. This is in agreement with previous measurements [36], and can be explained by the smoother surface of the samples due to the chemistry. The reduced surface roughness leads to a larger Kapitza resistance R_K, and therefore a smaller thermal transmittance. The second observation is that one sample pair, baseline 1, shows a higher thermal transmittance than the other three. It is not fully understood where this comes from, except that this was the very first surface chemistry and that the BCP took place at an elevated temperature. This was due to the fact that the chemistry was done in one large step instead of two, and as BCP is a strong exothermic reaction, created a temperature increase which then cause an increase of the etching rate and uneven etching. This would then lead to a larger surface roughness. Therefore, just as argued for the as-fabricated samples, the slightly larger surface roughness could explain the higher thermal transmittance. Also that all following baseline measurements done in two steps showed a lower thermal transmittance indicate that this might have been the cause. Nevertheless, a value of $190–260\,\mathrm{mW\,K^{-1}cm^{-2}}$ at 2 K is to be expected for niobium, and such spread was also observed in different measurements, and attributed to material properties such as RRR variations and surface properties like roughness [3,35]. Hence, our measurements are in agreement with literature values and we observe changes due to surface treatments on the same order of magnitude as expected. These results confirmed that the system is able to measure and quantify the impact of new surface treatments on the thermal transmittance.

4.2. SIS

The second surface treatment studied is the SIS structure, obtained by PEALD and subsequent annealing. Unfortunately, no baseline measurement of that sample pair, number 2, was available. The results obtained are compared to the average baseline value and shown in Fig. 7. The thermal transmittance of the as-deposited SIS sample is $(176.5 \pm 1.8\,(\mathrm{stat.}) \pm 21\,(\mathrm{sys.}))\,\mathrm{mW\,K^{-1}cm^{-2}}$, which is slightly lower than the average bare niobium but within the uncertainty. The value of the annealed SIS sample of $(195.9 \pm 1.0\,(\mathrm{stat.}) \pm 23\,(\mathrm{sys.}))\,\mathrm{mW\,K^{-1}cm^{-2}}$ is in agreement with the bare niobium average value. Given the thin films, an impact by the thermal conductivity was not expected unless a significant smaller value compared to niobium was to be found. As PEALD is a surface coating technique which mimics the surface topology, the surface roughness should prevail even for the thickness coated here. But the introduction of two interfaces, from Nb to AlN and from AlN to NbTiN, could have had the potential to increase the thermal resistance. From those two interfaces, the AlN to NbTiN interface was less likely to be an issue, as AlN is known to foster the properties of NbTiN, in particular for thin films [37], and therefore the heat transport across those two materials was not expected to be mitigated. Hence, the biggest impact was expected to come from the Nb-AlN interface, especially as the AlN is coated not on a bare niobium surface but onto the native oxide layer of niobium. This native oxide layer dissociates during the anneal, changing the interface, and it is further possible that the oxygen diffuses into the AlN and potentially change the thermal transmittance even further compared to the as-deposited value. The fact that the as-deposited SIS thermal transmittance is slightly smaller than the bare niobium thermal transmittance and also compared to the annealed SIS thermal transmittance indicates that there is a possible effect as described above, but it is well within the uncertainty of the measurement.

4.3. Mid-T

Based on Eq. (6), a decrease of the thermal conductivity due to the Mid-T heat treatment was expected, yet, a possible increase due to an improved Kapitza resistance was also possible. The result of the measurement is shown in Fig. 8. An increased thermal transmittance of the Mid-T heat treated sample of $(281.6 \pm 1.1\,(\mathrm{stat.}) \pm 34\,(\mathrm{sys.}))\,\mathrm{mW\,K^{-1}cm^{-2}}$ has been measured. This is contradicting the expectation that the thermal conductivity decreases as the purity of the material decreases, based on Eq. (6). Yet, the thickness of the layer is less than 1 µm, which has been shown by multiple studies [25,38], hence the impact might be negligible. As the thermal transmittance is also a measurement of the Kapitza resistance R_K, it possible that this improvement comes from a "more optimal" surface roughness caused by the altered oxide layer.

Other measurements done at DESY, such as B-mapping and f versus T measurements, performed on Mid-T heat treated cavities agree with an increased thermal transmittance. Multiple cavity tests of these two different types of measurements, whose results are both affected by the thermal transmittance, showed an effect which can be explained by an increased thermal transmittance.

5. Conclusion

The study presented here introduced a new experimental setup to obtain the thermal transmittance of samples at cryogenic temperatures. The first commissioning measurements of as-fabricated and baseline samples are in agreement with the literature and result to $(200.4 \pm 4\,(\mathrm{stat.}) \pm 24\,(\mathrm{sys.}))\,\mathrm{mW\,K^{-1}cm^{-2}}$ on average for the baseline at 2 K. The

Table 2
Overview of all results.

Status	K_0/mW K^{-1} cm^{-2}
As-fabricated	371 ± 0.5 (stat.) ± 36 (sys.)
As-fabricated	401 ± 0.6 (stat.) ± 39 (sys.)
Baseline 1	266.2 ± 3.0 (stat.) ± 32 (sys.)
Baseline 2	219.0 ± 3.8 (stat.) ± 26 (sys.)
Baseline 3	189.2 ± 0.9 (stat.) ± 22 (sys.)
Baseline 4	193.2 ± 0.7 (stat.) ± 23 (sys.)
Mid-T heat treated	281.6 ± 1.1 (stat.) ± 34 (sys.)
	271.4 ± 4.9 (stat.) ± 32 (sys.)
SIS as-deposited	176.5 ± 1.8 (stat.) ± 21 (sys.)
SIS annealed	195.9 ± 1.0 (stat.) ± 23 (sys.)
	195.8 ± 0.9 (stat.) ± 23 (sys.)

intent was then to study the thermal transmittance of multilayers, and how it relates to bare niobium and the measurement of an annealed SIS-sample show a thermal transmittance of $(195.9 \pm 1.0\,(\text{stat.}) \pm 23\,(\text{sys.}))\,\text{mW}\,\text{K}^{-1}\text{cm}^{-2}$, which falls into the range of normal bare niobium, and therefore SIS can be expected to behave thermally the same as niobium. The second treatment studied was the Mid-T heat treatment, which was motivated by preliminary findings in cavity tests and a fundamental relation between material purity and thermal conductance as described in Eq. (6). An increased thermal transmittance after the Mid-T heat treatment of $(281.6 \pm 1.1\,(\text{stat.}) \pm 34\,(\text{sys.}))\,\text{mW}\,\text{K}^{-1}\text{cm}^{-2}$ was measured, which indicates that the dominant effect is the altered oxide layer structure and less the reduced material purity. This is a significant increase compared to bare niobium, and its mechanism is still under investigation. This result also contributes to the investigation on the mechanism leading to the observation that Mid-T heat treated cavities have on average a lower quench field [20–22] compared to the standard surface treatment applied for the European XFEL [13]. A thermal quench, based on a negative thermal feedback, is ruled out due to these results, and a magnetic quench model as origin for the lower quench field is now the most likely.

CRediT authorship contribution statement

Marc Wenskat: Writing – original draft, Validation, Supervision, Resources, Project administration, Methodology, Investigation, Funding acquisition, Formal analysis, Conceptualization. **Leon King:** Software, Investigation, Formal analysis, Data curation. **Lasse Koch:** Formal analysis, Software, Visualization. **Cem Saribal:** Software, Methodology, Formal analysis. **Anton Lorf:** Formal analysis. **Isabel González Díaz-Palacio:** Writing – review & editing, Resources, Investigation. **Cornelius Martens:** Conceptualization. **Robert Zierold:** Writing – review & editing, Supervision, Resources. **Wolfgang Hillert:** Writing – review & editing, Supervision, Funding acquisition.

Declaration of competing interest

The authors declare that they have no known competing financial interests or personal relationships that could have appeared to influence the work reported in this paper.

Acknowledgments

The authors acknowledge the excellent support from DESY (Hamburg, Germany), a member of the Helmholtz Association HGF, especially for providing a niobium sheet and the access to the AMTF cryogenic test infrastructure - without this, the study would not have been possible. We thank R. Ghanbari (DESY) and J. Wolff (DESY) for the discussion on their respective cavity measurements. A special thanks to C. Antoine (CEA Saclay) and J. Amrit (LIMSI-CNRS) for the discussions and insights to the topic of thermal interface resistance. This work was supported by the BMBF, Germany under the research grants 05H21GURB2 and 05K22GUD.

Data availability

Data will be made available on request.

References

[1] H. Safa, An analytical approach for calculating the quench field in superconducting cavities. No. CEA-DAPNIA-SEA–96-05, 1996, https://accelconf.web.cern.ch/SRF95/papers/srf95c10.pdf.
[2] H. Padamsee, Influence of thermal conductivity on the breakdown field of niobium cavities, IEEE Trans. Magn. 21 (2) (1985) 149–152, http://dx.doi.org/10.1109/TMAG.1985.1063640.
[3] P. Dhakal, et al., Role of thermal resistance on the performance of superconducting radio frequency cavities, Phys. Rev. Accel. Beams 20 (3) (2017) 032003, http://dx.doi.org/10.1103/PhysRevAccelBeams.20.032003.
[4] Vincenzo Palmieri, et al., Evidence for thermal boundary resistance effects on superconducting radiofrequency cavity performances, Supercond. Sci. Technol. 27 (8) (2014) 085004, http://dx.doi.org/10.1088/0953-2048/27/8/085004.
[5] Kathleen Rempel Krafft, An investigation of thermal transport in superconducting cavities made of high thermal conductivity niobium, IEEE Trans. Magn. 19 (3) (1983) 1326–1329, http://dx.doi.org/10.1109/TMAG.1983.1062266.
[6] J. Amrit, M.X. François, Heat flow at the niobium-superfluid helium interface: Kapitza resistance and superconducting cavities, J. Low Temp. Phys. 119 (2000) 27–40, http://dx.doi.org/10.1023/A:1004604401306.
[7] C. Saribal, et al., Development of a thermal conductance instrument for niobium at cryogenic temperatures, in: 21th International Conference on RF Superconductivity (SRF'23), Grand Rapids, MI, USA, 25-30 June 2023, JACOW Publishing, Geneva, Switzerland, 2023, https://jacow.org/srf2023/papers/mopmb017.pdf.
[8] Pauli Virtanen, Ralf Gommers, Travis E. Oliphant, Matt Haberland, Tyler Reddy, David Cournapeau, Evgeni Burovski, Pearu Peterson, Warren Weckesser, Jonathan Bright, Stéfan J. van der Walt, Matthew Brett, Joshua Wilson, K. Jarrod Millman, Nikolay Mayorov, Andrew R.J. Nelson, Eric Jones, Robert Kern, Eric Larson, C.J. Carey, Ilhan Polat, Yu Feng, Eric W. Moore, Jake VanderPlas, Denis Laxalde, Josef Perktold, Robert Cimrman, Ian Henriksen, E.A. Quintero, Charles R. Harris, Anne M. Archibald, Antônio H. Ribeiro, Fabian Pedregosa, Paul van Mulbregt, SciPy 1.0 Contributors, SciPy 1.0: Fundamental algorithms for scientific computing in python, Nature Methods 17 (3) (2020) 261–272, http://dx.doi.org/10.1038/s41592-019-0686-2.
[9] M. Jergel, R. Stevenson, Static heat transfer to liquid helium in open pools and narrow channels, Int. J. Heat Mass Transfer 14 (12) (1971) 2099–2107, http://dx.doi.org/10.1016/0017-9310(71)90030-5.
[10] S.W. Van Sciver, Classical helium heat transfer, in: Helium Cryogenics, second ed., in: International Cryogenics Monograph Series, Springer, New York, NY, ISBN: 978-1-4419-9978-8, 2012, http://dx.doi.org/10.1007/978-1-4419-9979-5_5.
[11] S. Bousson, et al., Kapitza conductance and thermal conductivity of materials used for SRF cavities fabrication, in: 9th International Conference on RF Superconductivity (SRF'99), Santa Fe, NW, USA, 1-5 November 1999, JACOW Publishing, Geneva, Switzerland, https://accelconf.web.cern.ch/SRF99/papers/tup028.pdf.
[12] S. Aderhold, et al., Cavity Process, ILC HiGrade Reports ILC-HiGrade-Report-2010-005-1, 2010, https://www.ilc-higrade.eu/e83212/e99561/e99569/ILC-HiGrade-2010-005-1.pdf.
[13] D. Reschke, et al., Performance in the vertical test of the 832 nine-cell 1.3 GHz cavities for the European X-ray free electron laser, Phys. Rev. Accel. Beams 20 (4) (2017) 042004, http://dx.doi.org/10.1103/PhysRevAccelBeams.20.042004.
[14] M. Wenskat, et al., A new ultra-high vacuum furnace for SRF R & D, in: 21th International Conference on RF Superconductivity (SRF'23), Grand Rapids, MI, USA, 25-30 June 2023, JACOW Publishing, Geneva, Switzerland, 2023, https://accelconf.web.cern.ch/srf2023/papers/wepwb111.pdf.
[15] A. Gurevich, Maximum screening fields of superconducting multilayer structures, AIP Adv. 5 (1) (2015) http://dx.doi.org/10.1063/1.4905711.
[16] K. Takayuki, Multilayer coating for higher accelerating fields in superconducting radio-frequency cavities: a review of theoretical aspects, Supercond. Sci. Technol. 30 (2) (2016) 023001, http://dx.doi.org/10.1088/1361-6668/30/2/023001.
[17] A.-M. Valente-Feliciano, Superconducting RF materials other than bulk niobium: a review, Supercond. Sci. Technol. 29 (11) (2016) 113002, http://dx.doi.org/10.1088/0953-2048/29/11/113002.
[18] I. González.Díaz-Palacio, et al., Thermal annealing of superconducting niobium titanium nitride thin films deposited by plasma-enhanced atomic layer deposition, J. Appl. Phys. 134 (3) (2023) http://dx.doi.org/10.1063/5.0155557.
[19] V. Palmieri, Ruggero Vaglio, Thermal contact resistance at the Nb/Cu interface as a limiting factor for sputtered thin film RF superconducting cavities, Supercond. Sci. Technol. 29 (1) (2015) 015004, http://dx.doi.org/10.1088/0953-2048/29/1/015004.
[20] S. Posen, et al., Ultralow surface resistance via vacuum heat treatment of superconducting radio-frequency cavities, Phys. Rev. Appl. 13 (1) (2020) 014024, http://dx.doi.org/10.1103/PhysRevApplied.13.014024.

[21] F. He, et al., Medium-temperature baking of 1.3 GHz superconducting radio frequency single-cell cavity, Supercond. Sci. Technol. 34 (9) (2021) 095005, http://dx.doi.org/10.1007/s41605-020-00208-7.
[22] H. Ito, et al., Influence of furnace baking on QE behavior of superconducting accelerating cavities, Prog. Theor. Exp. Phys. 7 (2021) http://dx.doi.org/10.1093/ptep/ptab056.
[23] M. Wenskat, Vacancy-hydrogen dynamics and magnetic impurities during mid-t bake, in: 20th International Conference on RF Superconductivity (SRF'21), Grand Rapids, MI, USA, 28 June - 2 July 2021, JACOW Publishing, Geneva, Switzerland, 2021, https://accelconf.web.cern.ch/srf2021/papers/tuofdv03.pdf.
[24] R. Ghanbari, M. Wenskat, Technology Collaboration, Study of interstitial oxygen as a result of various surface treatments, in: TESLA Meeting, 5.-8. December 2023, Fermilab, Batavia, IL, USA, https://indico.fnal.gov/event/60446/contributions/277930/attachments/173280/234525/Talk_Wenskat.pdf.
[25] C. Bate, et al., Correlation of srf performance to oxygen diffusion length of medium temperature heat treated cavities, 2024, http://dx.doi.org/10.48550/arXiv.2407.07779, arXiv preprint arXiv:2407.07779.
[26] G.D.L. Semione, et al., Niobium near-surface composition during nitrogen infusion relevant for superconducting radio-frequency cavities, Phys. Rev. Accel. Beams 22 (10) (2019) 103102, http://dx.doi.org/10.1103/PhysRevAccelBeams.22.103102.
[27] G.D.L. Semione, et al., Temperature-dependent near-surface interstitial segregation in niobium, J. Phys.: Condens. Matter. 33 (26) (2021) 265001, http://dx.doi.org/10.1088/1361-648X/abf9b7.
[28] H. Padamsee, The technology of nb production and purification, in: 2nd International Conference on RF Superconductivity (SRF'84), Geneva, Switzerland 23 - 27. July 1984, JACOW Publishing, Geneva, Switzerland, https://accelconf.web.cern.ch/srf84/papers/srf84-21.pdf.
[29] A. Ramiere, S. Volz, J. Amrit, Thermal resistance at a solid/superfluid helium interface, Nat. Mater. 15 (5) (2016) 512–516, http://dx.doi.org/10.1038/nmat4574.
[30] I.N. Adamenko, I.M. Fuks, Roughness and thermal resistance of the boundary between a solid and liquid helium, Sov. Phys. JETP 32 (6) (1971) 1123–1129.
[31] Mingming Yu, et al., Study on the interstitial oxygen diffusion to understand the reduction of cryogenic RF loss for the superconducting radio-frequency niobium cavities, Supercond. Sci. Technol. 37 (10) (2024) 105014, http://dx.doi.org/10.1088/1361-6668/ad7645.
[32] Alena Prudnikava, et al., In-situ synchrotron x-ray photoelectron spectroscopy study of medium-temperature baking of niobium for SRF application, Supercond. Sci. Technol. 37 (7) (2024) 075007, http://dx.doi.org/10.1088/1361-6668/ad4825.
[33] Y. Bozhko, et al., Test stands for testing serial XFEL accelerator modules 2011, Adv. Cryog. Eng. B 57, 1110–1107, http://dx.doi.org/10.1063/1.4707030.
[34] J. Schaffran, et al., Design parameters and commissioning of vertical inserts used for testing the XFEL superconducting cavities, in: AIP Conference Proceedings, Vol. 1573, American Institute of Physics, 2014, http://dx.doi.org/10.1063/1.4860705, (1).
[35] A. Aizaz, et al., Thermal design studies of niobium SRF cavities, in: 13th International Conference on RF Superconductivity (SRF'07), Beijing, China, 14-19 October 2007, JACOW Publishing, Geneva, Switzerland, 2023, https://accelconf.web.cern.ch/srf2007/TALKS/WE102_TALK.pdf.
[36] J. Amrit, C.Z. Antoine, Kapitza resistance cooling of single crystal (111) niobium for superconducting rf cavities, Phys. Rev. Spec. Topics— Accel. Beams 13 (2) (2010) 023201, http://dx.doi.org/10.1103/PhysRevSTAB.13.023201.
[37] T. Shiino, et al., Improvement of the critical temperature of superconducting NbTiN and NbN thin films using the AlN buffer layer, Supercond. Sci. Technol. 23 (4) (2010) 045004, http://dx.doi.org/10.1088/0953-2048/23/4/045004.
[38] E.M. Lechner, et al., RF surface resistance tuning of superconducting niobium via thermal diffusion of native oxide, Appl. Phys. Lett. 119 (8) (2021) http://dx.doi.org/10.1063/5.0059464.